Bacterial adaptation to cold: Conservation of a short J-domain co-chaperone and its protein partners in environmental proteobacteria

Lana Weber, Atar Gilat, Nathanael Maillot, Deborah Byrne, Pascal Arnoux, Marie-thérèse Giudici-orticoni, Vincent Méjean, Marianne Ilbert, Olivier Genest, Rina Rosenzweig, et al.

Received: 8 March 2023 | Accepted: 20 July 2023

DOI: 10.1111/1462-2920.16478

RESEARCH ARTICLE

ENVIRONMENTAL MICROBIOLOGY Applied Microbiology International

Bacterial adaptation to cold: Conservation of a short J-domain co-chaperone and its protein partners in environmental proteobacteria

Lana Weber[1] | **Atar Gilat**[2] | **Nathanael Maillot**[1] | **Deborah Byrne**[3] | **Pascal Arnoux**[4] | **Marie-Thérèse Giudici-Orticoni**[1] | **Vincent Méjean**[1] | **Marianne Ilbert**[1] | **Olivier Genest**[1] | **Rina Rosenzweig**[2] | **Sébastien Dementin**[1]

[1]Laboratory of Bioenergetics and Protein Engineering (BIP UMR 7281), Aix-Marseille University, French National Center for Scientific Research (CNRS), Marseille, France

[2]Department of Chemical and Structural Biology, Weizmann Institute of Science, Rehovot, Israel

[3]Protein Expression Facility, Aix-Marseille University, French National Center for Scientific Research (CNRS), IMM FR3479, Marseille, France

[4]Institute of Biosciences and Biotechnologies of Aix-Marseille (BIAM UMR7265), Aix-Marseille University, French Alternative Energies and Atomic Energy Commission (CEA), French National Center for Scientific Research (CNRS), Saint Paul-Lez-Durance, France

Correspondence
Sébastien Dementin, Aix-Marseille University, French National Center for Scientific Research (CNRS), BIP UMR 7281, IMM, 31 Chemin Joseph Aiguier, 13402 Marseille, France.
Email: dementin@imm.cnrs.fr

Present addresses
Lana Weber, Architecture et Fonction des Macromolécules Biologiques (AFMB UMR 7257), French National Center for Scientific Research (CNRS), Aix-Marseille University, Marseille, France; and Nathanael Maillot, Institut Micalis, UMR 1319, INRAE, Jouy-en-Josas, France.

Funding information
Agence Nationale de la Recherche, Grant/Award Numbers: ANR-16-CE11-0002-01, ANR-19-CE44-0018; Aix-Marseille University; Centre National de la Recherche Scientifique

Abstract

Bacterial genomes are a huge reservoir of genes encoding J-domain protein co-chaperones that recruit the molecular chaperone DnaK to assist protein substrates involved in survival, adaptation, or fitness. The *atc* operon of the aquatic mesophilic bacterium *Shewanella oneidensis* encodes the proteins AtcJ, AtcA, AtcB, and AtcC, and all of them, except AtcA, are required for growth at low temperatures. AtcJ is a short J-domain protein that interacts with DnaK, but also with AtcC through its 21 amino acid C-terminal domain. This interaction network is critical for cold growth. Here, we show that AtcJ represents a subfamily of short J-domain proteins that (i) are found in several environmental, mostly aquatic, β- or γ-proteobacteria and (ii) contain a conserved PX_7W motif in their C-terminal extension. Using a combination of NMR, biochemical and genetic approaches, we show that the hydrophobic nature of the tryptophan of the *S. oneidensis* AtcJ PX_7W motif determines the strong AtcJ–AtcC interaction essential for cold growth. The AtcJ homologues are encoded by operons containing at least the *S. oneidensis atcA*, *atcB*, and *atcC* homologues. These findings suggest a conserved network of DnaK and Atc proteins necessary for low-temperature growth and, given the variation in the *atc* operons, possibly for other biological functions.

INTRODUCTION

In the environment, bacteria face biotic and abiotic variations to which they must constantly adapt. Among the physicochemical parameters, temperature is probably one of the most crucial. The transition to low temperatures influences many cellular processes (membrane fluidity, water viscosity, enzyme kinetics, RNA metabolism, etc.) on which the survival of the cell depends. The psychrophilia or psychrotolerance of some bacteria is based on mechanisms acting at several levels, both environmental, physiological and molecular but which depend on the bacterium, its lifestyle and its temperature preference (Barria et al., 2013; Casanueva et al., 2010; de Maayer et al., 2014; Zhang & Gross, 2021). The cold shock response is composite. It is the result of adaptive responses leading to regulation of gene expression through changes in DNA topology, transcription, RNA metabolism (RNA folding and degradation), increased membrane fluidity, improved translation (ribosome and translation factors) and protein folding (Zhang & Gross, 2021). For example, it is well documented that a specific metabolism must be set up at low temperature to adapt the lipid composition of the membrane necessary for its integrity and functioning. In addition, low temperature may cause stabilisation of secondary structures of the mRNA, which can disrupt translation and result in a defect of protein synthesis (Barria et al., 2013; Casanueva et al., 2010; de Maayer et al., 2014; Zhang & Gross, 2021). Thus, the cold response involves the induction of the production of proteins specifically involved in mRNA management such as ribonucleases to degrade misfolded mRNA, or cold-shock proteins whose role is to prevent the formation of unwanted secondary structures (Barria et al., 2013; Casanueva et al., 2010; de Maayer et al., 2014; Zhang & Gross, 2021).

Bacteria of the genus *Shewanella* are aquatic (seawater or freshwater) and are therefore able to survive and even grow in cold environments. Some species of *Shewanella* are identified as psychrophilic but some, mesophilic, whose optimal growth temperature is above 20°C can grow at temperatures well below 10°C (Hau & Gralnick, 2007; Hwang et al., 2019; Lemaire et al., 2019; Lemaire et al., 2020). This is the case for *S. oneidensis* which has an optimum growth rate around 30°C but grows, although more slowly, in a temperature range of 4–37°C (Abboud et al., 2005; Jeong et al., 2006). Compared to cells grown at 22°C, *S. oneidensis* cells grown at low temperature have particular phenotypic characteristics, such as a smaller diameter and a tendency to filamentation, which are accompanied, as explained before, by a change in the production of certain proteins and a major modification of the composition of cellular lipids (Abboud et al., 2005). A study also demonstrated that survival of *S. oneidensis* at low temperature depended on excision of a cryptic prophage in a subpopulation of cells in which increased ability to form attached biofilm ensures prolonged survival under cold (Zeng et al., 2016).

Recently, our lab has identified an operon in *S. oneidensis* essential for growth at low temperature, named *atc* for adaptation to cold (Maillot et al., 2019). This operon which is constitutively expressed in the temperature range of 7–37°C encodes the four proteins AtcJ, AtcA, AtcB, and AtcC (Figure 1A). The deletion of the genes of this operon has no effect on the growth of *S. oneidensis* at the optimal temperature of 28°C but causes a growth defect at 7°C, except for Δ*atcA* which shows no growth defect at any temperature. AtcJ is a J-domain containing protein (JDP). JDPs, named as such on the basis of their homology with the *E. coli* prototype DnaJ, represent a large family of proteins that interact with and regulate the activity of the molecular chaperone DnaK (Hsp70 in eukaryotes). All proteins from this family contain the J-domain, a ∼70 amino acids domain composed of four helices forming a hairpin. The flexible loop that connects helices II and III bears the conserved HPD motif that determines the interaction with DnaK (Figure 1B; Kampinga & Craig, 2010; Craig & Marszalek, 2017; Rosenzweig et al., 2019; Barriot et al., 2020). Basically, JDPs' function is to address proteins that are partially folded, misfolded or aggregated to DnaK. Binding of JDPs to DnaK triggers allosteric changes in DnaK that result in ATPase activity stimulation (Mayer, 2018). The specificity of the substrates to be delivered to DnaK is determined by the additional domains of JDPs. Alternatively, JDPs can localise DnaK/Hsp70 to cellular compartments where chaperone activity is needed (Balchin et al., 2020; Mayer, 2021; Mayer & Gierasch, 2019; Serlidaki et al., 2020). Nevertheless, their role is certainly underestimated if one considers the vast diversity of additional domains found in bacterial JDPs (Barriot et al., 2020).

AtcJ is unique in that it is a short 94 amino-acids JDP constituted of a J-domain flanked by a C-terminal extension of only 21 amino acids. The interaction of AtcJ with DnaK through its J-domain is essential for cold growth. Indeed, production of AtcJ harbouring a mutation on the HPD motif which prevents interaction with DnaK, in the Δ*atcJ* strain, did not restore growth at low temperature (Maillot et al., 2019). On the basis of bacterial two-hybrid and isothermal titration calorimetry experiments, we have previously shown that the small terminal extension is responsible for the strong interaction of AtcJ with the AtcC protein (Kd of ∼ 10nM) (Figure 1B). Complementation of the Δ*atcJ* strain with a plasmid expressing *atcJ* truncated from this extension failed to restore growth at low temperature, suggesting that the AtcJ–AtcC interaction is essential for growth. In addition, we showed that AtcC also interacts with AtcB (Maillot et al., 2019). The mechanism by which the AtcB and AtcC proteins promote growth at low-

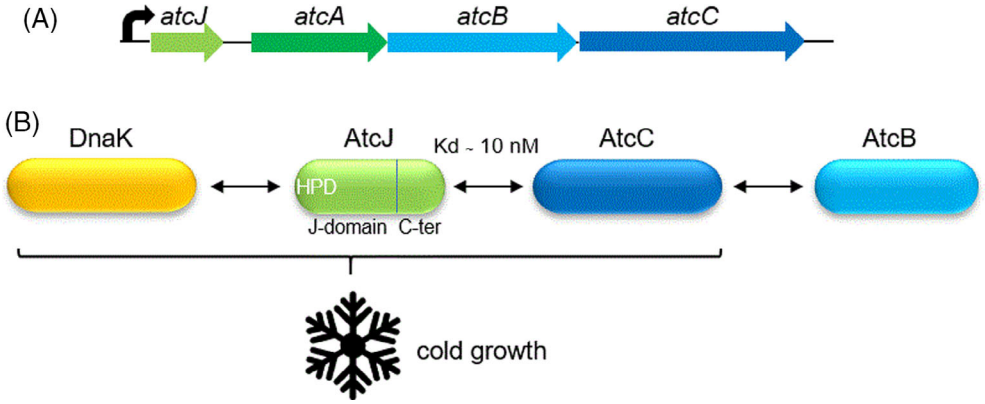

FIGURE 1 Overview of the *atc* operon from *S. oneidensis* and functional protein interaction network. (A) Scheme of the *atc* operon. (B) AtcJ binds DnaK through the HPD motif of its J-domain, and binds AtcC via its 21 amino acids C-terminal extension. In addition, AtcC interacts with AtcB. The AtcJ-DnaK and AtcJ–AtcC interactions are crucial for growth at low temperature.

temperature in *S. oneidensis* is unknown. AtcB is toxic when overproduced in *S. oneidensis* or *E. coli* at the optimal growth temperatures of 28 and 37°C, respectively. This is probably the result of a reduced level of transcription, as suggested by an in vivo *lacZ* reporter experiment in *E. coli* (Maillot et al., 2021). Moreover, co-purification and in vitro transcription/translation assays showed that AtcB interacts with the core RNA polymerase (α, α, β′, β, and ω subunits) and probably inhibits it (Maillot et al., 2021). The relevance of these observations regarding the role of Atc proteins in cold growth remains to be demonstrated. Nevertheless, one can anticipate a function in recruiting DnaK to modulate RNA polymerase activity and allow efficient transcription of key genes under cold conditions. Because *S. oneidensis* also possesses another Hsp70 homologue (HscA), one cannot rule out the possibility that the Atc proteins also recruit it.

In this paper, we determine that AtcJ is part of a subfamily of short JDPs encoded in *atc* operons found in several environmental, mostly aquatic, β- and ɣ-proteobacteria genomes. This family is hallmarked by a conserved PX_7W motif located in an alpha helix of the C-terminal extension. The hydrophobic and aromatic properties of the conserved tryptophan at position 89 of AtcJ from *S. oneidensis* are critical for strong AtcJ–AtcC interaction. Accordingly, the suppression of this interaction in vivo by introducing a non-hydrophobic residue at this position on the *S. oneidensis* chromosome causes a growth defect at low temperature.

EXPERIMENTAL PROCEDURES

Growth conditions and strains

The *E. coli* and the *S. oneidensis* strains used in this study were listed in Table S1, respectively and grown at the desired temperature in Luria Bertani (LB) rich medium: bacto-tryptone (10 g/L), yeast extracts (5 g/L), NaCl (5 g/L), pH 7.4. Agar at 1.5% is added to this medium for solid media (LB-agar). When selection is required, antibiotics were added at the following concentrations: chloramphenicol 25 μg/mL, ampicillin 50 μg/mL, kanamycin 50 μg/mL, rifampicin 10 μg/mL and streptomycin 100 μg/mL. For growth monitoring at 7–9°C and 28°C, cells were grown under agitation (180 rpm) in 50 mL Erlenmeyer flasks containing 10 mL of LB medium in the presence of chloramphenicol and 0.2% arabinose.

Transformations of *E. coli* strains were performed using the heat shock method, with cells made competent by cold $CaCl_2$ treatment. *S. oneidensis* strains were transformed by conjugation according to the procedure already described (Baraquet et al., 2009).

The *S. oneidensis* strains containing a mutated *atcJ* gene coding for $AtcJ_{W89S}$ and $AtcJ_{W89R}$ were constructed as follows. Two fragments of 500 bp upstream and downstream of the codon to be mutated in *atcJ*, respectively, were generated by PCR using the chromosome of *S. oneidensis* MR-1 as a template with specific primers (Table S2). These two PCR products overlap on a 27-base pair region and are centered on the mutated codon. They were cloned into the suicide vector pKNG101 (Baraquet et al., 2009) and digested with BamHI and SpeI using the NEBuilder HiFi DNA Assembly kit (New England Biolabs Inc). The two obtained plasmids (pKNG101-$atcJ_{W89S}$ and pKNG101-$atcJ_{W89R}$, Table S3) contain the 1000 bp region of the chromosome of *S. oneidensis* MR-1 centered on the W89S or W89R mutations in the *atcJ* gene.

S. oneidensis MR-1 was transformed by the obtained plasmids pKNG101-$atcJ_{W89S}$ or pKNG101-$atcJ_{W89R}$ (Table S3) by conjugation and the mutations were introduced in the chromosome by homologous recombination according to the procedure described before (Baraquet et al., 2009).

Plasmid constructions

For two-hybrid experiments, plasmids pT18-AtcJ coding for AtcJ fused to the C-terminal extremity of the T18 domain of the adenylate cyclase and pT25-AtcC coding for fusion of AtcC to the C-terminus of the T25 domain of the adenylate cyclase described before (Maillot et al., 2019) were used. The mutations P81A, W89S, W89F, W89Y, W89R W89E, W89Q, W89L, and W89M in T18-AtcJ were constructed by site-directed mutagenesis using QuickChange kit (Agilent) for W89S or Q5® Site-Directed Mutagenesis Kit (New England Biolabs Inc) for the other mutants according to the manufacturer instructions. The primers and plasmids used are described in Tables S2 and S3, respectively.

For complementation experiments, the pBAD33 and pBAD33-AtcJ plasmids described before were used (Maillot et al., 2019). The mutations W89S, W89F, and W89R in pBAD33-AtcJ were constructed by site-directed mutagenesis using Q5® Site-Directed Mutagenesis Kit (New England Biolabs Inc) according to the manufacturer instructions. The primers and plasmids used are described in Tables S2 and S3, respectively.

The pET-AtcJ and pET-AtcC plasmids were used to produce WT AtcJ-6His, and WT AtcC-6His (Maillot et al., 2019). The pET-AtcJ plasmid was used as a template to produce the W89S-, W89L-, W89F-, and W89R-AtcJ-6His mutants by site-directed mutagenesis using QuickChange kit (Agilent) for W89S or Q5® Site-Directed Mutagenesis Kit for the other mutants (New England Biolabs Inc) according to the manufacturer instructions. The primers and plasmids used are described in Tables S2 and S3, respectively.

Bacterial two-hybrid assay

E. coli strain BTH101 was co-transformed with the different plasmid constructs pT25-atcC and pT18-atcJ (WT or mutated; Table S3). Transformants were selected on LB-agar medium containing ampicillin and kanamycin. After 48 h of incubation at 28°C, about 10 clones were cultured overnight at 28°C in 24-well plates containing 1 mL of LB, both antibiotics and 1 mM IPTG. After measuring OD_{600nm}, 100 μL of 10-fold diluted cells were distributed in wells of a 96-well microplate and lysed by addition of 10 μL of Popculture Reagent solution (EMD Milipore Corp.) containing 1 mg/mL of lysozyme. After 15 min of incubation at room temperature, 100 μL of Z buffer (75 mM Na_2HPO_4, 10 mM NaH_2PO_4, 5 mM KCl, 0.5 mM $MgSO_4$, 50 mM β-mercaptoethanol, pH 7) was added to each well. The β-galactosidase activity was measured by monitoring the optical density at 420 nm with a TECAN microplate reader, after addition by the automatic injector of the reader of 40 μL of 4 mg/mL ONPG to each well. Experiments were performed in triplicate. The slope of the traces was used to calculate the β-galactosidase activity as already described (Baaziz et al., 2017).

Control of cellular protein amounts

To check that the same amount of wild-type and mutant of T18-AtcJ proteins were produced, the *E. coli* MG1655 strain was transformed with pT18-AtcJ (WT or mutant). The transformants were grown overnight at 37°C in the presence of 1 mM IPTG. The total protein extracts from the same amount of cells were heat-denatured, loaded on SDS-PAGE, transferred by western blot and revealed with anti-AtcJ antibody as described before (Maillot et al., 2019).

The amount of cellular AtcJ proteins (WT and mutants) produced from chromosome or plasmid was checked after cells wer grown at $OD_{600nm} \approx 2$. The total protein extracts from the same amount of cells were heat-denatured, loaded on SDS-PAGE, transferred by western blot and revealed with anti-AtcJ antibody as described before (Maillot et al., 2019).

We checked the amount of DnaK and DnaJ in the WT, Δ*atcJ*, $atcJ_{W89S}$, and $atcJ_{W89R}$ *S. oneidensis* strains. The cells were grown at exponential phase ($OD_{600nm} = 4–5$), the total protein extracts from the same amount of cells were heat-denatured, loaded on SDS-PAGE, transferred by western blot and revealed with anti-DnaK antibody raised against two immunogenic peptides of *S. oneidensis* DnaK (Genscript). The same extracts were used to determine the amount of DnaJ, detection was carried out with commercial anti-DnaJ from *E. coli* antibody (Enzo Life Sciences, Inc.).

Protein purification

Strains of *E. coli* BL21 (DE3) containing the different pET plasmid constructs (Table S3) were cultured at 37°C to $OD_{600nm} = 0.8$. The production of AtcJ, $AtcJ_{W89S}$, $AtcJ_{W89F}$, $AtcJ_{W89R}$, and $AtcJ_{W89L}$ proteins was induced by addition of 1 mM IPTG and incubation for 2 h at 37°C. For AtcC, induction of protein production was achieved by addition of 1 mM IPTG and incubation for 20 h at 16°C. Cells were collected by centrifugation for 15 min at 5000 rpm at 4°C. The pellets were resuspended in 20 mL of 20 mM Tris-HCl (pH 7.5). A second centrifugation of 15 min at 11,000 rpm at 4°C was performed and the pellets were resuspended in 20 mL of buffer A (20 mM phosphate buffer, 500 mM NaCl, 10% glycerol, pH 7.4) containing 20 mM imidazole and DNase. The cells were then broken by 2 passages in a French press and the cell debris was removed by centrifugation performed at 11,000 rpm for 15 min at 4°C. After ultracentrifugation at 45,000 rpm, for 1 h at 4°C, the supernatants were

filtered (0.45 μm membrane) and loaded on a HisTrap HP column (GE Healthcare) using an AKTA Pure apparatus (GE Healthcare). After two washes with buffer A containing 20 and 50 mM imidazole, the proteins were eluted with buffer A containing 100, 200, and 500 mM imidazole. Fractions containing the proteins of interest were then pooled and concentrated (volume < 5 mL) using Amicon Centrifugal Filters (Milipore). Samples were loaded onto a HiLoad 16/600 Superdex 200 pg gel filtration column (GE Healthcare), with the AKTA Pure system (GE Healthcare) in buffer B (50 mM Tris-HCl, 100 mM KCl, 10% glycerol, 1mM DTT) to increase protein purity and change the buffer of samples. Protein concentrations were measured from $OD280_{nm}$ measurements using the theoretical molar extinction coefficient determined by protein sequence (Protparam Expasy).

NMR spectroscopy

All NMR experiments were recorded at 25°C on a Bruker 800 MHz AVANCE NMR spectrometer equipped with a cryoprobe. Isotopically labelled AtcJ was grown in M9 H2O media supplemented with $^{15}NH_4Cl$ and ^{13}C-glucose as the sole nitrogen and carbon source, respectively. Labelled AtcJ and AtcC were purified according to the procedure described above. Backbone ^{1}H, ^{15}N, and ^{13}C assignments were obtained on a sample of 2 mM [$^{1}H/^{15}N/^{13}C$]-labelled AtcJ (in 50 mM Hepes, pH 7.0, 50 mM KCl) using a set of 3D HNCA, HNCACB, HNCACO, and HNCO triple resonance experiments. Spectra were processed with NMRPipe (Delaglio et al., 1995) and analysed using CCPNMR (Vranken et al., 2005). The structural model of AtcJ was generated with CS-Rosetta, based on ^{15}N, $^{13}C\alpha$, $^{13}C\beta$, $^{13}C'$, and ^{1}HN chemical shifts using a standard CS-Rosetta protocol. The resulting 10 lowest energy structures (of 3000) displayed a backbone root mean square deviation (rmsd) of <1.5 Å from the lowest energy structure (Shen et al., 2008).

Circular dichroism

Purified AtcJ, $AtcJ_{W89S}$, $AtcJ_{W89F}$, and $AtcJ_{W89R}$ proteins were desalted against 20 mM phosphate buffer pH 7.4 using ZEBA SPIN columns (Thermo Scientific). The samples were diluted to a concentration of 15 μM and the circular dichroism spectra were recorded with a JASCO-815 spectrophotometer at 25°C in a 1 mm cell.

Isothermal titration calorimetry

The AtcJ and AtcC proteins were dialyzed overnight at 4°C in buffer B to avoid discrepancies from buffer mismatch. ITC experiments were performed at 25°C using the MicroCal PEAQ-ITC (Malvern). In total, 207 μM of ligands ($AtcJ_{WT}$, $AtcJ_{W89S}$, $AtcJ_{W89F}$, $AtcJ_{W89R}$, and $AtcJ_{W89L}$) were titrated against 36 μM of AtcC in the ITC cell with a constant stirring speed of 750 rpm. A total of 19 injections were performed with an initial injection of 0.4 μL followed by 18 injections of 2 μL with a spacing time of 150 seconds. Duplicates were performed for each measurement, except for $AtcJ_{WT}$. The heat generated by the dilution effect of the last injections was removed from the isothermal data as the fitted offset control. The data were fitted using a "One Set of Sites" model in the PEAQ-ITC Analysis Software.

Accession numbers

AtcJ NMR chemical shifts have been deposited in the Biological Magnetic Resonance Data Bank (BMRB), accession number 51734.

RESULTS

AtcJ belongs to a subgroup of short JDPs containing a conserved PX_7W motif and found in several environmental β- or γ-proteobacteria

Barriot et al. showed that AtcJ from *S. oneidensis* (AtcJ_son) belongs to a group of J-domain proteins that have the feature of being short in size (Barriot et al., 2020). In their paper aimed at describing the biodiversity of J-domain proteins in bacteria and phages, they identified in a selection of 1709 genomes representative of bacterial diversity a total of 105 short JDPs with sizes ranging from 54 to 100 amino acids. We used these 105 sequences to identify AtcJ homologues. Although there are some examples of JDPs that do not have the canonical HPD motif (Kluck et al., 2002; Walsh et al., 2004), we discarded the 11 sequences that do not contain a proper HPD sequence. Then, we aligned the remaining 94 sequences using the Multalin website (Corpet, 1988). The results are represented using the ESPript 3.0 website (Robert & Gouet, 2014) with an imposed similarity score of 0.7 (Figure S1). Two groups can be differentiated on the basis of the location of the HPD motif, either in the N-terminal or C-terminal half of the proteins. Except for a region corresponding to residues 53-60 (VKKAYEVL) in *S. oneidensis* (Uniprot code Q8EFW5), no overall similarity is detected. Nevertheless, AtcJ_son appears to be part of a subgroup of 34 sequences in which P81 and W89 in the C-terminal extension are highly conserved (red and green insets in Figure S1). Therefore, this subgroup can be identified by this conserved

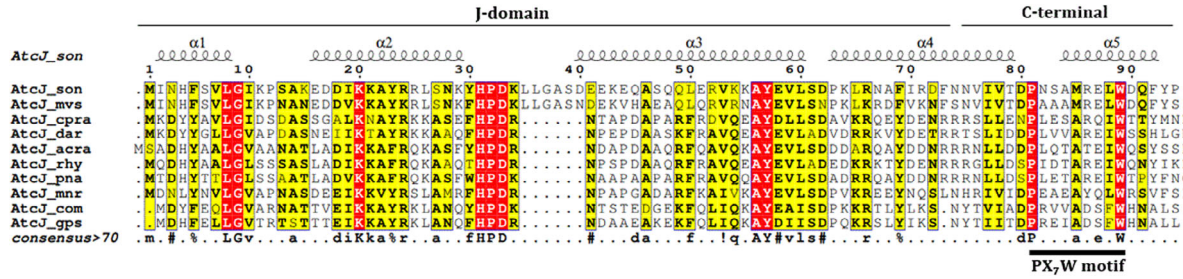

FIGURE 2 Identification of a conserved PX_7W motif in the subfamily of very short JDPs to which AtcJ belongs. Amino acid alignement of 10 homologues representative of the AtcJ superfamily, performed with Multalin and represented using Espript 3.0 (similarity score of 0.7). The strictly conserved residues are in white and framed under a red background. The residues considered as highly similar are framed under a yellow background. The secondary structure depicted is based on the AlphaFold structure model of AtcJ from *S. oneidensis*. The organisms are *S. oneidensis* (son), *Moritella viscosa* (mvs), *Collimonas pratensis* Ter91 (cpra), *Dechloromonas aromatica* (dar), *Acidovorax* sp. RAC01 (acra), *Rhodoferax koreense* (rhy), *Polaromonas naphtalenivorans* (pna), *Massilia* sp NR 4-1 (mnr), *Colwellia* sp. MT41 (com), *Paraglaciecola psychrophila* (gps).

PX_7W motif. In two sequences, the PX_7W motif is degenerated: the tryptophan is replaced by an alanine in the sequence from *Janthinobacterium* sp. B9-8 (Uniprot code A0A109RWT6) and the proline is replaced by an alanine in the JDP from *Candidatus Thiodictyon syntrophicum* (Uniprot code A0A2K8U395). These two sequences were nevertheless kept in the subgroup. On the contrary, the JDPs from *Solidesulfovibrio magneticus* RS-1 (Uniprot code C4XM59) and from *Verrucomicrobium* sp. GAS474 (Uniprot code A0A1H2E3L7) which contains neither the proline nor the tryptophane were discarded from the group. For clarity, an alignment performed with a selection of 10 sequences from this subgroup is presented in Figure 2.

The members of the PX_7W motif-containing JDP subgroup identified in Figure S1 are all found in environmental organisms belonging to the β- or γ-proteobacteria classes (Table 1). Most of the strains are aquatic (marine water, freshwater, sludge, sediments). A minority (~27%) was collected from soil samples. The β-proteobacteria are mostly from the *Burkholderiales* order and a minority belong to the *Nitrosomonadales* and *Rhodocyclales* orders. The γ-protobacteria are essentially from the *Alteromonadales* order. Considering their psychrophilia or psychrotolerance, the information that we have found in the literature is reported in Table 1. It appears that in all the organisms for which the question has been raised, an ability to survive or even grow at low temperature is described.

We further investigated the phylogenetic distribution and the extent of deviation from the PX_7W motif in JDPs from this subgroup by exploring the KEGG database (Kanehisa, 2019; Kanehisa et al., 2021; Kanehisa & Goto, 2000) (see additional data 1 and Figures S2–S4). From this analysis, we conclude that, although it may be degenerated in a few cases, the PX_7W motif appears as a hallmark of a subgroup of short JDPs homologous to AtcJ_son, that are restricted to several species of β- or γ-proteobacteria classes.

Exogenous AtcJs complement the cold growth defect of the *S. oneidensis* Δ*atcJ* strain

We studied the functionality of some of these AtcJ homologs by assessing their ability to complement the low-temperature growth defect of the Δ*atcJ* mutant of *S. oneidensis*. We selected three proteins from the 10 representative sequences in Figure 2, that is, from *Collimonas pratensis* Ter91 (Cpra), *Rhodoferax koreense* (Rhy) and *Paraglaciecola psychrophila* (Gps). After codon optimization, the genes were synthesised and cloned into pBAD33 for arabinose inducible expression. The plasmids were introduced in *S. oneidensis* Δ*atcJ* by conjugation and the growth at 7°C in the presence of 0.2% arabinose of two independent clones was compared to that of the WT and Δ*atcJ* strains. Figure S5 shows that the genes from Cpra and Rhy restored growth of the Δ*atcJ* strain but with a significant delay compared to WT. The gene from Gps did not restore cold growth. Whether these delays or non-complementation are the result of a protein production defect in *S. oneidensis* and/or low affinity for *S. oneidensis* obligatory interactants for cold growth (DnaK and AtcC) remains to be determined.

The conserved tryptophan of the AtcJ PX_7W motif is essential for AtcC binding in *S. oneidensis*

The interaction between AtcJ and AtcC from *S. oneidensis* was suggested to be mediated by the C-terminal extension of AtcJ (residues N74 to P94) (Maillot et al., 2019) which contains the conserved

TABLE 1 Description and phylogenetic distribution of the 32 organisms containing a gene coding for AtcJ homologue identified by Barriot et al. among 1709 genomes representative of bacterial biodiversity.

UniProt protein Id	Lenght (aa)	Group	Conserved pattern	Organism	Class	Order	Habitat/collection location	Psychrophilia/ psychrotolerance	References
A0A090KA95	96	JDP-short	PX_7W	*Moritella viscosa* (mvs)	*γ-proteobacteria*	*Alteromonadales*	Marine water (salmon pathogen)	Psychrophilic, infection at < 10°C	Tunsjø et al. (2007)
A0A0A1FDV1	92	JDP-short	PX_7W	*Collimonas arenae* strain Cal35	*β-proteobacteria*	*Burkholderiales*	Soil	N A	Uroz et al. (2014)
A0A0K1J5X0	95	JDP-short	PX_7W	*Azoarcus* sp. CIB	*β-proteobacteria*	*Rhodocyclales*	Soil, rice endophyte	N A	Fernández et al. (2014)
A0A0K1JYK5	97	JDP-short	PX_7W	*Massilia* sp. NR 4-1 (mnr)	*β-proteobacteria*	*Burkholderiales*	Soil	N A	Myeong et al. (2016)
A0A0S2JDU8	86	JDP-short	PX_7W	*Colwellia* sp. MT41 (com)	*γ-proteobacteria*	*Alteromonadales*	Marine water	Psychrophilic and barophilic	Peoples et al. (2020)
A0A127QR12	92	JDP-short	PX_7W	*Collimonas pratensis* strain Ter291 (cpra)	*β-proteobacteria*	*Burkholderiales*	Soil, mycophage	N A	Song et al. (2015)
A0A1B3PN06	98	JDP-short	PX_7W	*Acidovorax* sp. RAC01 (acra)	*β-proteobacteria*	*Burkholderiales*	Marine water (algal phycosphere)	N A	Fixen et al. (2016)
A0A1D8RZ81	90	JDP-short	PX_7W	*Colwellia* sp. PAMC 20917	*γ-proteobacteria*	*Alteromonadales*	Marine water	Psychrophilic, range 4–15°C	Kim et al. (2018)
A0A1P8K3R8	92	JDP-short	PX_7W	*Rhodoferax* sp. DCY110 (*R. koreense*) (rhy)	*β-proteobacteria*	*Burkholderiales*	Sludge	Growth at 4°C observed	Farh et al. (2017)
A0A1P8KAC7	91	JDP-short	PX_7W	*Rhodoferax saidenbachensis* strain DSM 22694	*β-proteobacteria*	*Burkholderiales*	Freshwater	Growth at 4°C observed	Farh et al. (2017)
A0A1Y0N561	91	JDP-short	PX_7W	*Curvibacter* sp. AEP1-3	*β-proteobacteria*	*Burkholderiales*	Marine water (metazoan associated)	N A	Ulrich et al. (2022)
A0A240U302	94	JDP-short	PX_7W	*Acidovorax* sp. NA3	*β-proteobacteria*	*Burkholderiales*	Soil	N A	Singleton et al. (2009)
A1TS52	93	JDP-short	PX_7W	*Acidovorax citrulli* AAC00-1	*β-proteobacteria*	*Burkholderiales*	Cucurbit pathogen	N A	Fessehaie and Walcott (2005)
A1VSC3	91	JDP-short	PX_7W	*Polaromonas naphthalenivorans* CJ2 (pna)	*β-proteobacteria*	*Burkholderiales*	Aquatic, sediment	Growth observed between 4 and 25°C	Jeon et al. (2004)
B1KPF4	94	JDP-short	PX_7W	*Shewanella woodyi* ATCC 51908	*γ-proteobacteria*	*Alteromonadales*	Marine water	Growth at 4°C observed	Makemson et al. (1997)
C7RKF6	92	JDP-short	PX_7W	*Candidatus* Accumulibacter *phosphatis* clade IIA str. UW-1	*β-proteobacteria*	Unclassified	Freshwater	N A	Petriglieri et al. (2022)
D7DID8	93	JDP-short	PX_7W	*Methylotenera versatilis* 301	*β-proteobacteria*	*Nitrosomonadales*	Freshwater	Range 4–30°C	Kalyuzhnaya et al. (2012)
D9SFD9	96	JDP-short	PX_7W	*Gallionella capsiferriformans* ES-2	*β-proteobacteria*	*Nitrosomonadales*	Freshwater	Growth at 6°C observed	Emerson and Moyer (1997)
G0AG67	92	JDP-short	PX_7W	*Collimonas fungivorans* Ter331	*β-proteobacteria*	*Burkholderiales*	Plant roots associated	Growth observed between 4°C and 20–30°C	de Boer et al. (2004)

(Continues)

TABLE 1 (Continued)

UniProt protein Id	Lenght (aa)	Group	Conserved pattern	Organism	Class	Order	Habitat/collection location	Psychrophilia/ psychrotolerance	References
K0I1S2	98	JDP-short	PX_7W	*Acidovorax* sp. KKS102	*β-proteobacteria*	*Burkholderiales*	Soil	N A	Kimbara et al. (1988)
K6YY10	86	JDP-short	PX_7W	*Paraglaciecola psychrophila* 170 (gps)	*γ-proteobacteria*	*Alteromonadales*	Arctic marine water	Psychrophilic, range 4–15°C	Zhang et al. (2006)
Q087F8	94	JDP-short	PX_7W	*Shewanella frigidimarina* NCIMB 400	*γ-proteobacteria*	*Alteromonadales*	Marine water	Range 0–25°C	Bowman et al. (1997)
Q125J9	91	JDP-short	PX_7W	*Polaromonas* sp. JS666	*β-proteobacteria*	*Burkholderiales*	Groundwater	N A	Coleman et al. (2002)
Q12JR0	94	JDP-short	PX_7W	*Shewanella denitrificans* OS217	*γ-proteobacteria*	*Alteromonadales*	Marine water	Range 4–30°C	Brettar et al. (2002)
Q479W6	92	JDP-short	PX_7W	*Dechloromonas aromatica* RCB (dar)	*β-proteobacteria*	*Rhodocyclales*	River sludge	N A	Coates et al. (2001)
Q486D3	86	JDP-short	PX_7W	*Colwellia psychrerythraea* 34H	*γ-proteobacteria*	*Alteromonadales*	Marine arctic sediment	Psychrophilic, range 1–10°C	Methé et al. (2005)
Q5NZ33	92	JDP-short	PX_7W	*Azoarcus aromaticum* EbN1	*β-proteobacteria*	*Rhodocyclales*	Freshwater/soil	N A	Rabus et al. (2019)
Q8EFW5	94	JDP-short	PX_7W	*Shewanella oneidensis* MR-1 (son)	*γ-proteobacteria*	*Alteromonadales*	Marine and freshwater	Range 4–37°C	Jeong et al. (2006)
R4YNE7	89	JDP-short	PX_7W	*Oleispira antarctica* strain RB-8	*γ-proteobacteria*	*Oceanospirillales*	Antarctic sea water	Psychrophilic, optimum growth at 2–4°C	Yakimov et al. (2003)
W0VBX5	96	JDP-short	PX_7W	*Janthinobacterium agaricidamnosum* NBRC 102515 = DSM 9628	*β-proteobacteria*	*Burkholderiales*	Fungus pathogen	N A	Lincoln et al. (1999)
A0A109RWT6	92	JDP-short	PX_7A	*Janthinobacterium* sp. B9-8	*β-proteobacteria*	*Burkholderiales*	Sewage	Range 4–37°C	Xu et al. (2019)
A0A2K8U395	89	JDP-short	AX_7W	*Candidatus Thiodictyon syntrophicum* strain Cad16T	*γ-proteobacteria*	*Chromatiales*	Freshwater	Range 5–25°C	Peduzzi et al. (2012)

Abbreviation: N A, not addressed in literature.

PX_7W motif. To confirm this, we recorded ^{1}H-^{15}N HSQC NMR binding experiments between purified ^{15}N-isotopically labelled AtcJ and unlabeled AtcC. Addition of two-fold excess of AtcC caused severe peak broadening to the C-terminal region of AtcJ (residues 73–94), indicating binding (Figure 3A). To obtain structural information for the C-terminal region of AtcJ_son, we derived secondary structures from the assigned backbone ($^{13}C\alpha$, $^{13}C\beta$, $^{13}C'$, ^{15}N, and ^{1}HN) NMR chemical shifts of AtcJ, using the program TALOS^{+} (Shen

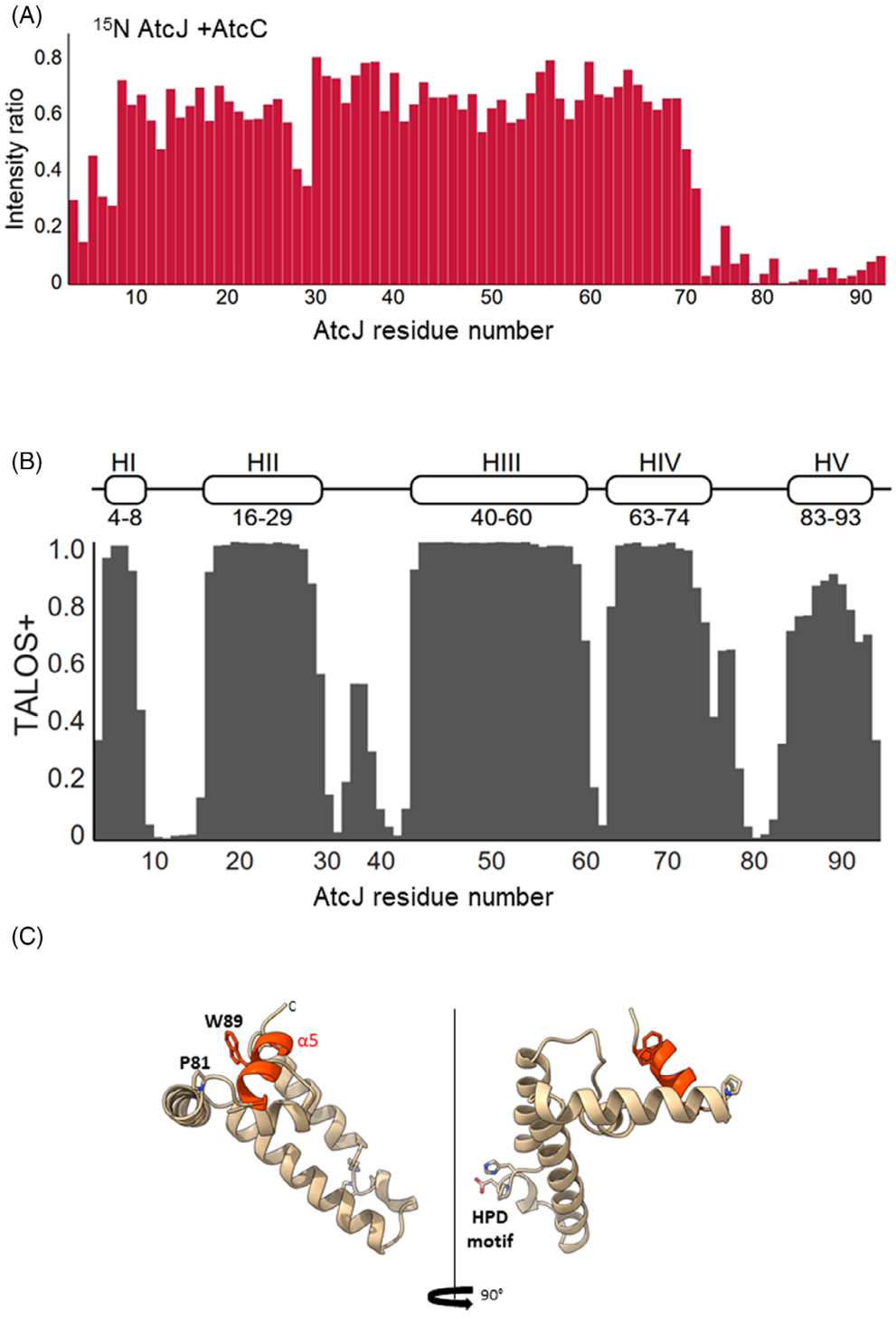

FIGURE 3 Interaction of AtcJ with AtcC and model structure of AtcJ determined by NMR. (A) Intensity changes (I/I_0) of ^{15}N labeled AtcJ upon addition of AtcC. AtcC binds to residues 73–93 in the C-terminal domain of AtcJ. (B) Secondary structure of AtcJ derived by TALOS^{+} from the backbone NMR $^{13}C\alpha$, $^{13}C\beta$, $13C'$, ^{15}N, and ^{1}HN chemical shifts. (C) Structure of AtcJ derived by CS-Rosetta based on NMR restraints. The HPD motif is essential for interaction with DnaK. Conserved proline (P81) and tryptophan (W89) on the C-terminal extention of AtcJ are indicated. Helix α5 in orange contains conserved tryptophan (W89) the indole ring of which is surface exposed.

et al., 2009). AtcJ_son presented a characteristic JDP fold, with the J-domain composed of four helices and the surface-exposed H31-P32-D33 motif in a loop connecting helices 2 and 3. The C-terminal extension (residues N74 to P94) was partially structured as an alpha helix (α5), starting from S83 within the conserved PX_7W motif and ending at Y93 (Figure 3B). We next used the NMR chemical shifts as an input for CS-Rosetta (Lange et al., 2012) to calculate a structural model for AtcJ_son (Figure 3C). The calculated structures presented a characteristic JDP fold, with helices 2 and 3 antiparallel to one another and connected by a loop with the conserved Hsp70-binding HPD motif. The C-terminal helix 5 was present in a number of different orientations relative to the J-domain, further indicating that this domain moves freely in solution and does not form contact with the J-domain.

Using AlphaFold software (Mirdita et al., 2022), we modelled the structures of the nine other homologs containing an intact PX_7W motif already selected above. According to their high similarity, the J-domains of the nine other modelled structures have the same overall folding as AtcJ_son as shown by a structure overlay achieved with ChimeraX software (Goddard et al., 2018; Pettersen et al., 2021; Figure S6). Their C-terminal extension also partially folds as an alpha helix but starts from the conserved proline of the PX_7W motif while the NMR structure suggests that it starts two residues after. Moreover, the orientations of the C-terminal extensions containing the alpha helix 5 strongly differ depending on the protein (Figure S6), suggesting that, as supported by NMR data, they may adopt a different orientation relative to their core N-terminal domain.

We used site directed mutagenesis to assess the role of the conserved P81 and W89 residues in the *S. oneidensis* AtcJ–AtcC interaction. As a tool for screening, we used the bacterial two-hybrid assay that has allowed us to demonstrate this interaction (Maillot et al., 2019). It is based on the reconstitution of the T18 and T25 catalytic domains of the adenylate cyclase of *Bordetella pertussis* (Battesti & Bouveret, 2012; Karimova et al., 1998). AtcJ was fused to the T18 domain and AtcC to the T25 domain. When produced together in an adenylate cyclase-deleted *E. coli* strain, the high level of β-galactosidase activity, caused by the induction of expression of the *lac* operon as a result of cAMP production by the reconstituted adenylate cyclase, reflects the interaction between AtcJ and AtcC (Maillot et al., 2019). We, therefore, constructed the T18-$AtcJ_{P81A}$ and T18-$AtcJ_{W89S}$ fusions and their interaction with T25-AtcC was measured (Figure 4). The β-galactosidase activity measured with T18-$AtcJ_{P81A}$ was identical to that of WT. On the contrary, the activity was dramatically low with T18-$AtcJ_{W89S}$, suggesting a possible role of this residue for interaction with AtcC.

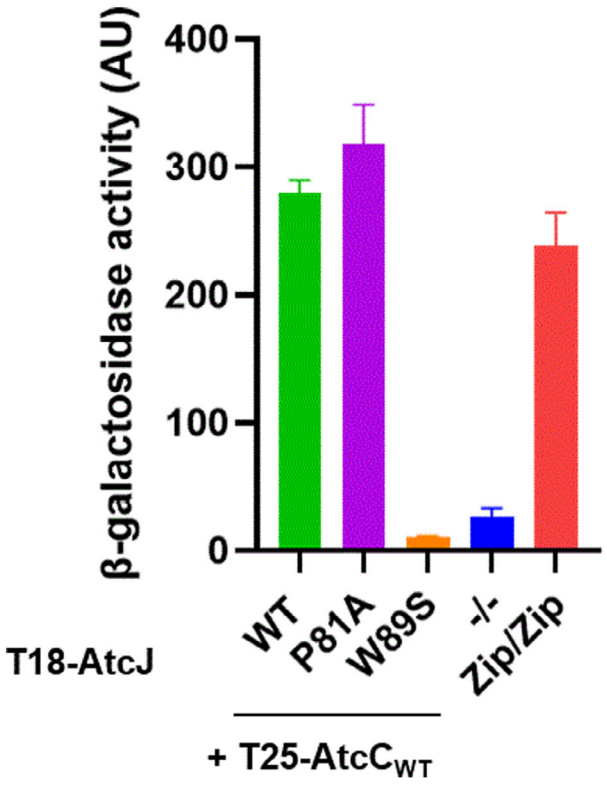

FIGURE 4 Effect of mutations on the conserved PX_7W motif of AtcJ on interaction with AtcC assessed by bacterial two-hybrid assay. *E. coli* BTH101 strain co-transformed as indicated with the T18 and T25 plasmids coding for protein fusion between T18 and AtcJ (WT and mutants), and protein fusion between T25 and AtcC. A positive control (Zip/Zip, pUT18C-zip with pKT25-zip) and a negative control (-/-, empty vectors) were also included in the experiment. Cells were grown overnight at 28°C. β-galactosidase activity was measured as explained in the Methods section. The data from three replicates are shown as mean ± SD.

The hydrophobic nature of the residue at position 89 is critical for the AtcJ–AtcC interaction in *S. oneidensis*

We then evaluated by bacterial two-hybrid assay how the nature of the side chain of this residue at position 89 affects the AtcJ–AtcC interaction by replacing it by hydrophobic aromatic (Phe and Tyr) or hydrophobic non-aromatic (Leu and Met), polar (Ser and Gln), positively charged (Arg) and negatively charged (Glu) residues on the T18-AtcJ fusion. Figure 5A shows that the interaction is conserved only when the side chain of the residue is hydrophobic (T18-$AtcJ_{W89F}$, T18-$AtcJ_{W89Y}$, T18-$AtcJ_{W89L}$, and T18-$AtcJ_{W89M}$ fusions). To ensure that the absence of interaction observed with non hydrophobic residues is not the result of decreased production of T18-AtcJ fusions, their amount was evaluated by Western Blot with an anti-AtcJ antibody (Maillot et al., 2019). Figure S7 shows that when produced in *E. coli*, the T18 fusions that do not display interaction with AtcC ($AtcJ_{W89S}$, $AtcJ_{W89Q}$,

AtcJ$_{W89R}$, and AtcJ$_{W89E}$) are detected in amounts comparable to those of fusions that do interact (AtcJ$_{WT}$, AtcJ$_{W89F}$, and AtcJ$_{W89Y}$), suggesting that the low level of β-galactosidase activity measured is the result of a defect in the interaction of AtcJ with AtcC, rather than of low protein production.

To check that the W89 mutations did not result in major secondary structure changes that render the proteins nonfunctional for interaction with AtcC, we examined the secondary structures of wild type AtcJ and three selected mutants by circular dichroism. We thus purified a set of mutants: AtcJ$_{W89F}$, for which the interaction with AtcC is conserved, and AtcJ$_{W89S}$ and AtcJ$_{W89R}$ mutants for which the interaction is not observed. The three mutants as well as AtcJ$_{WT}$ were overproduced and purified by affinity chromatography according to the protocols described before (Maillot et al., 2019) and recalled in Materials and Methods. The CD spectrum obtained for AtcJ$_{WT}$ is typical of a protein with a high proportion of α-helices. The overlap of the spectra obtained for AtcJ$_{WT}$ and the three mutants indicates a similar spectral signature, without major changes in secondary structure (Figure S8).

To quantitatively characterise the interaction between WT or mutated AtcJ and AtcC, we performed isothermal titration calorimetry using purified AtcC as described before (Maillot et al., 2019; Figures 5B and S9). A dissociation constant (Kd) of 12.2 nM for the WT protein was measured, a value similar to what was obtained previously (Maillot et al., 2019). With AtcJ$_{W89F}$, a similar Kd of 14 ± 1.6 nM was measured, which is consistent with bacterial two-hybrid results reporting a strong interaction between the two proteins. While the two-hybrid experiment suggests a level of interaction comparable to the WT protein, a Kd of 48 ± 4 nM is measured with the AtcJ$_{W89L}$ mutant. In the case of W89S and W89R mutations of AtcJ, and as suggested by the two-hybrid experiment, a dramatic loss of affinity is observed. For AtcJ$_{W89S}$, a Kd of 6.6 ± 1.4 μM was determined, while for AtcJ$_{W89R}$, no interaction was detected. These experiments confirm that a hydrophobic residue at position 89 of AtcJ is essential to ensure high affinity for AtcC and that the aromatic character of this residue seems to be a factor improving the interaction.

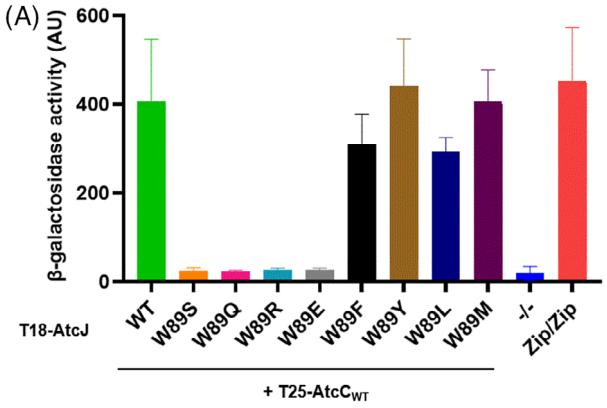

(B)

Samples	Kd (nM)
AtcC + AtcJ$_{WT}$	12.2
AtcC + AtcJ$_{W89S}$	6600 ± 1380
AtcC + AtcJ$_{W89F}$	14.4 ± 1.6
AtcC + AtcJ$_{W89R}$	No binding
AtcC + AtcJ$_{W89L}$	48 ± 4

FIGURE 5 Impact of the nature of the residue at position 89 of *S. oneidensis* AtcJ on the interaction with AtcC. (A) Bacterial two-hybrid assay showing that a hydrophobic residue at position 89 is crucial for AtcJ–AtcC interaction. *E. coli* BTH101 strain co-transformed as indicated with the T18 and T25 plasmids coding for protein fusion between T18 and AtcJ (WT and mutants), and protein fusion between T25 and AtcC. A positive control (Zip/Zip, pUT18C-zip with pKT25-zip) and a negative control (-/-, empty vectors) were also included in each experiment. Cells were grown overnight at 28°C. β-galactosidase activity was measured as explained in the Methods section. The data from three replicates are shown as mean ± SD. (B) Dissociation constants of the AtcJ–AtcC interaction measured using ITC. Binding assays were performed at 25°C with 36 μM AtcC and 207 μM AtcJ (WT and mutants). Experiments were performed in duplicate, except for AtcC + AtcJ$_{WT}$ which was already measured (Maillot et al., 2019) and repeated once in this study.

Mutations of W89 that abolish the AtcJ–AtcC interaction in *S. oneidensis* cause a growth defect at low temperatures

The growth at low temperature of the *S. oneidensis* strains in which the gene encoding AtcJ carries the W89S and W89R mutations on the chromosome was tested and compared with that of wild-type and Δ*atcJ* strains. We first observed that the two-point mutations do not affect the growth of the bacteria at the optimal growth temperature of 28°C, as observed when *atcJ* is deleted (Maillot et al., 2019). The growth curves are similar to those of the wild-type strain (Figure 6A). Regarding low temperature (9°C), Figure 6B shows that the WT strain starts growing after a <48 h lag. The Δ*atcJ* strain did not grow during the period of the experiment (196 h) in accordance with what was observed before (Maillot et al., 2019). In the case of the *atcJ*$_{W89S}$ strain, a significant growth delay was observed compared to WT, with a lag of ∼80 h. The *atcJ*$_{W89R}$ strain did not grow. Production of AtcJ$_{WT}$ from a plasmid rescued the growth of the Δ*atcJ*, *atcJ*$_{W89S}$, and *atcJ*$_{W89R}$ strains (Figure 6B). To rule out the possibility that these effects were the result of protein production defects caused by the point mutations, we checked the cellular amount of the AtcJ proteins by western blot using an anti-AtcJ antibody as described before (Maillot et al., 2019). The experiment could not be performed at low temperature because the strains Δ*atcJ* and *atcJ*$_{W89R}$ do not grow under this condition. We thus performed the experiment at the optimal temperature of

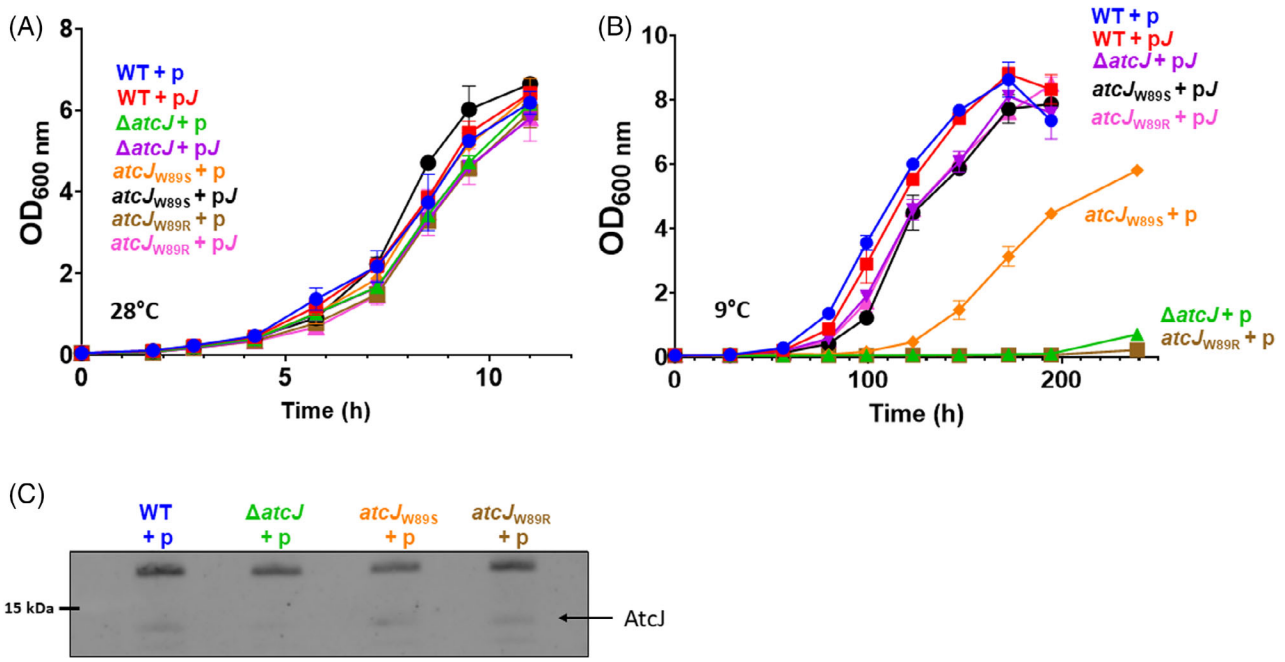

FIGURE 6 Growth of *S. oneidensis* WT and mutant (Δ*atcJ*, $atcJ_{W89S}$ and $atcJ_{W89R}$) strains at 28 and 9°C. Cultures are conducted in LB medium in the presence of chloramphenicol and 0.2% arabinose. After initial growth at 28°C, strains were diluted to $OD_{600nm} = 0.05$, and were incubated at 28°C (A) or 9°C (B) with shaking. The strains contains pBAD33 either empty (+p) or expressing atcJ (+p*J*). Absorbance was measured over time. The data from two replicates are shown as mean ± SD. The amount of AtcJ proteins produced at 28°C was checked by analysing protein extracts by Western blot using anti-AtcJ antibody (C).

28°C where all the strains have comparable growth kinetics. The low level of AtcJ protein produced from chromosome made it poorly detectable, nevertheless, the $AtcJ_{WT}$, $AtcJ_{W89S}$, and $AtcJ_{W89R}$ proteins appear to be produced in the same amount (Figure 6C). As an additional control, we studied the effect of overproduction from plasmid of AtcJ (WT, W89S, W89F, or W89R) on the cold growth of Δ*atcJ*. In agreement with what was observed when produced from chromosome, overproduction of $AtcJ_{W89R}$, which does not interact with AtcC, does not restore cold growth of Δ*atcJ* (Figure S10A). Cold growth of Δ*atcJ* overproducing $AtcJ_{W89S}$ compares to that of the WT strain and Δ*atcJ* overproducing $AtcJ_{W89F}$, a result that apparently contradicts the growth delay observed with the $atcJ_{W89S}$ strain. As determined by ITC experiments, this mutation significantly affects the ability of AtcJ to bind AtcC, but still allows residual interaction. Therefore, the overproduction of $AtcJ_{W89S}$ from plasmid may have compensated the weak interaction with AtcC and allowed the Δ*atcJ* strain to grow as rapidly as the WT strain. At 28°C, these strains had comparable growth kinetics and produced comparable amounts of the Atc proteins, which supports the idea that point mutations have no effect on the stability of the protein (Figures S10B and S10C).

The deletion of *dnaK* and *dnaJ* in *E. coli* is associated with increase in the cellular concentrations of the other remaining molecular chaperones and proteases (Calloni et al., 2012; Fauvet et al., 2021). We thus wondered whether deletion or mutations of *atcJ* caused a change in the amount of DnaK and DnaJ in the *S. oneidensis* Δ*atcJ*, $atcJ_{W89S}$, and $atcJ_{W89R}$ strains. Using antibodies raised against DnaK and DnaJ (Figures S11A and S11B), we determined by western blot that the amount of DnaK and DnaJ in these three strains is comparable to that of WT.

The genes encoding AtcJ are in synteny with *atcA*, *atcB*, and *atcC*

We have shown previously that *atcJ*, *atcA*, *atcB*, and *atcC* of *S. oneidensis* are part of the same operon (Maillot et al., 2019; Figure 1). We further investigated this aspect by examining the genetic environment of the genes coding for AtcJ homologues identified in Figure S1 using the KEGG website (Kanehisa, 2019; Kanehisa et al., 2021; Kanehisa & Goto, 2000). We observed that they were always localised upstream of at least three other genes which appear to be transcriptionally linked since, as in *S. oneidensis*, the genes overlap and/or have very short intergenic regions. This is also the case for the genes coding for AtcJ homologues mentioned above in which the PX_7W motif is degenerated. For clarity, we present in Figure 7 the genetic environment of the 10 *atcJ* homologues selected above.

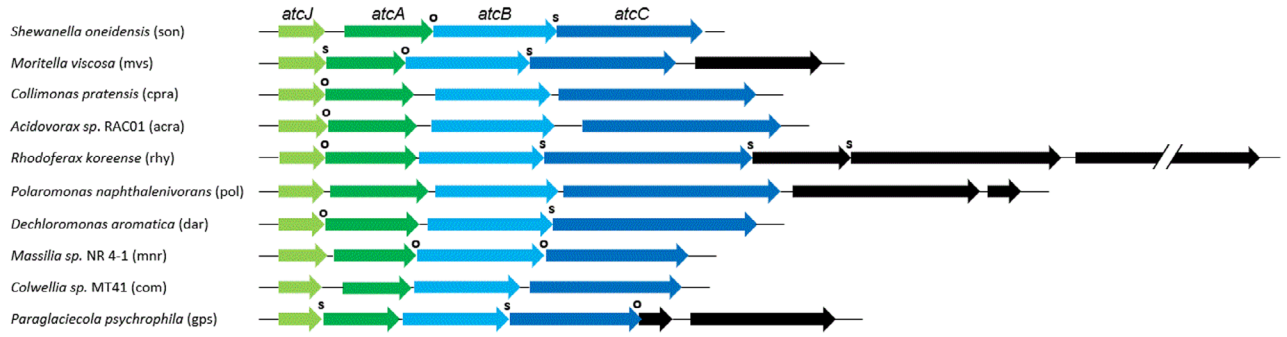

FIGURE 7 Genetic environment of genes coding for AtcJ homologues from 10 representative organisms as annotated in the KEGG database. The size of genes and intergenic sequences (thin lines) is indexed to that of *atcJ* from *S. oneidensis* (285 bp). Two contiguous genes with overlapping bases or short intergenic sequences (<18 pb) are labeled o and s, respectively. In black are represented the genes of unknown function that are possibly in transcriptional link with *atcC* equivalents. The third gene downstream of the equivalent of *atcC* in *Rhodoferax koreense* is predicted to be 5531 bp and has, therefore, been truncated for representation.

To determine whether these downstream genes encode equivalents to *S. oneidensis* AtcA, AtcB, and AtcC, respectively, we aligned the corresponding protein sequences from the 10 organisms selected above (including *S. oneidensis*) using the Multalin interface. The results are represented using the ESPript 3.0 website with an imposed similarity score of 0.7. Concerning the gene downstream of *atcJ* (i.e., *atcA*), the alignment of the corresponding proteins reveals only one strictly conserved aspartyl residue (D28 of AtcA from S. *oneidensis*; Figure S12). Nevertheless, many motifs (from a unique amino acid to a sequence of five residues) display a high degree of similarity. Remarkably, all sequences have a C-terminal end rich in acidic amino acids. Using the AlphaFold software, we modelled the structure of the 10 corresponding proteins, and selected the rank 1 models which we overlaid using the ChimeraX 1.3 software. According to the structural model, AtcA_son is organised into two domains (Figure 8A, upper panel). The N-terminal domain is globular, composed of 7 alpha helices and 3 3_{10}-helices, one of which being the N-terminal extension of alpha-helix 6. The C-terminal domain, starting at residue G132, contains the region rich in acidic amino acids and appears globally disordered. The nine other structural models also show a 2-domain organisation with the N-terminal domains overlapping with that of AtcA_son and a highly disordered C-terminal domain which corresponds to the acidic region. In five cases (AtcA from *Acidovorax* sp. RAC01, *Rhodoferax koreense*, *Polaromonas naphtalenivorans*, *Dechloromonas aromatica* and *Collimonas pratensis* Ter91), this region contains a C-terminal extension of 20-23 amino-acids that folds into an alpha helix (Figure 8A, lower panel). Therefore, in these organisms, the first gene downstream of *atcJ* encodes a protein structurally related to AtcA_son which has the distinctive feature of having a long, apparently disordered acidic C-terminal domain.

Considering the proteins encoded by the second gene downstream of *atcJ*, that is, *atcB* in *S. oneidensis*, the sequence alignments show many similar motifs and few strictly conserved residues (Figure S13). The 3D model of AtcB_son suggests a fifteen alpha helix organization. Alpha Helices 6 and 10 have a 3_{10}-helix extension in their C-terminal end. A long unstructured loop separates helices 10 and 11 (Figure 8B, upper panel). The overlay of the AlphaFold structural models reveals a remarkable folding similarity (Figure 8B, lower panel). The structural models diverge only in the number and arrangement of residues between helices 10 and 11, and after helix 13 where strong structural heterogeneity is predicted. Thus, again, in these organisms, the second gene downstream of *atcJ* encodes a protein structurally close to AtcB_son, suggesting a functional similarity.

Although AtcA and AtcB equivalents have comparable sizes, the selected potential AtcC equivalents have sizes ranging from 269 to 444 amino acids. Sequence alignment shows that despite low sequence identity, many similar motifs are present, especially in the N-terminal part (i.e., approximately up to residue 200 of AtcC_son; Figure S14). The AlphaFold generated model structure of AtcC_son consists of two globular domains connected by a long alpha helix (helice α7) (Figure 8C, upper panel). The superposition of the 3D models suggests a remarkable structural similarity of the N-terminal domains, from helix 1–6. After helix 7, the structures diverge strongly (Figure 8C, lower panel). So, in these organisms, the third gene downstream of *atcJ* encodes a protein structurally related to AtcC_son at the level of the N-terminal domain.

The same modellings performed on the 23 other organisms producing a very short JDP of the AtcJ subgroup from Figure S1 lead to the same observations regarding the potential structure conservation of the three proteins encoded downstream of *atcJ*.

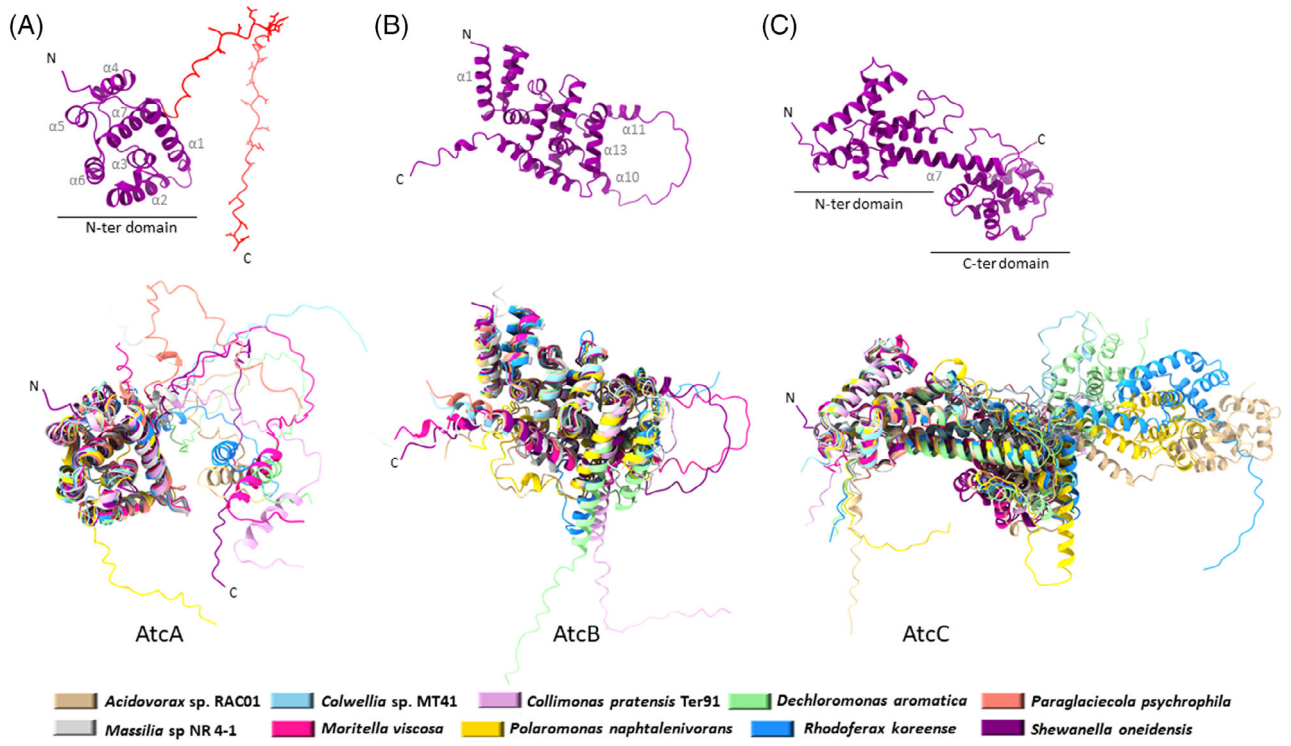

FIGURE 8 Prediction and overlay of the structures of AtcA, AtcB, and AtcC homologues. Structural prediction of Atc proteins from the 10 representative organisms were obtained using the AlphaFold interface. The rank 1 structure models were selected. Overlay of the 10 AlphaFold structure models of Atc proteins were realised with ChimeraX software. Upper panels: Atc proteins from *S. oneidensis*. Lower panels: overlay of the predicted structures of Atc proteins from 10 representative organisms. (A) AtcA. The disordered acidic C-terminal domain of *S. oneidensis* AtcA is shown in red in the upper panel. The side chains of aspartate and glutamate residues are depicted. (B) AtcB. (C) AtcC.

To make sure that the synteny observed between *atcJ*, *atcA*, *atcB*, and *atcC* is specific, we carefully examined the genetic environment of the genes encoding JDPs that are not in the AtcJ_son subgroup in Figure S1. In all cases, the gene is followed or preceded by genes that have no particular homology with *atcA*, *atcB*, or *atcC*. Thus, this suggests that *atcJ* is consubstantial with the other three genes *atcA*, *atcB*, and *atcC* in an operonic organization. These genes encode for proteins that seem highly structurally related (Figure 8), suggesting a conserved concerted function of the four proteins in collaboration with DnaK.

DISCUSSION

The growth of *S. oneidensis* at low temperature depends on the *atc* operon containing the *atcJ*, *atcA*, *atcB*, and *atcC* genes. The *atcJ* gene codes for a short JDP which interacts with DnaK via its J-domain and with AtcC through its C-terminal extension of 21 amino acids. This interaction network is essential for cold growth (Maillot et al., 2019). By studying the distribution of AtcJ in the bacterial biodiversity, we discovered that it is part of a subfamily of homologous short JDPs found in Gram-negative organisms from the β- and γ-proteobacteria classes (Table 1). These Jdps are always encoded with three other genes that seem in synteny and which encode for proteins predicted to be structurally related to AtcA, AtcB and AtcC from *S. oneidensis*. This JDP subfamily is hallmarked by a conserved PX_7W motif in the C-terminal extension. The hydrophobic and aromatic nature of the tryptophan residue ensures a high affinity for the interaction between AtcJ and AtcC. In line with this, when this interaction is disrupted in vivo by replacing this Trp by a non hydrophobic residue, the ability of *S. oneidensis* to grow at low temperatures is dramatically affected.

The β-proteobacteria possessing this probable operon are mostly from the *Burkholderiales* order and a minority belongs to the *Nitrosomonadales* and *Rhodocyclales* orders. The γ-protobacteria are essentially from the *Alteromonadales* or *Aeromonadales* orders. The habitat of the majority of these organisms is aquatic but some of them were collected from soil samples and/or are pathogens, parasites or symbionts of eukaryotic organisms.

Although AlphaFold modelizations on AtcJ homologues suggest the proline of the PX_7W motif is at the start of the C-terminal alpha helix, our NMR study on the protein from *S. oneidensis* rather suggests that the helix starts two residues after. We identified a few AtcJ homologues in which the Pro is replaced by Ala. In the two-hybrid experiment we performed, we indeed showed that the replacement of the proline (P81 in *S. oneidensis* AtcJ) is not critical to ensure interaction

with AtcC (Figure 4), so the role of this conserved residue is unclear. However, we show that the surface-exposed conserved tryptophan (W89 in *S. oneidensis* protein) in this helix is essential to ensure the high affinity of AtcJ for AtcC (Kd in the order of 10 nM). The interaction is severely affected when this residue is replaced by a hydrophilic or charged residue as judged by two-hybrid assay and isothermal titration calorimetry experiments. The hydrophobicity of this residue is crucial and its aromatic property seems to significantly increase the affinity for AtcC. An indole ring does not seem to be specifically required since interaction with AtcC is observed when the tryptophan is replaced by a phenylalanine or a tyrosine as shown by a two-hybrid assay. Strikingly, the affinity of AtcJ for AtcC is almost identical when Trp is replaced by Phe. One can consider that this aromatic residue is involved in non-covalent interactions with AtcC through Pi–Pi stacking with aromatic side-chains (McGaughey et al., 1998) or cation-Pi stacking with positively charged residue (Dougherty, 1996, 2013; Gallivan & Dougherty, 1999). However, the fact that non-aromatic leucine residue at position 89 is sufficient to ensure high affinity, suggests instead that AtcJ and AtcC interact via an intermolecular apolar bond. Interestingly, we did not identify any homologs in which the tryptophan is replaced by another aromatic residue, although such mutations (W89F and W89Y) have no impact on the interaction. It may be that tryptophan provides a particular advantage, for interaction with AtcC or other functions, that will have to be discovered.

When the $AtcJ_{W89R}$ and $AtcJ_{W89S}$ mutations which abolish or impair, respectively, the interaction with AtcC, are transferred into the chromosome of *S. oneidensis*, the ability of the organism to grow at low temperature is affected. At 9°C, the $atcJ_{W89R}$ strain does not grow, demonstrating that the interaction is essential for cold growth (Figure 6). The $atcJ_{W89S}$ strain grows at this temperature, but with a significant delay compared to the WT strain (Figure 6) although the affinity of $AtcJ_{W89S}$ for AtcC is decreased by a factor of 550 compared to WT protein. We hypothesize that, although weak, the affinity of $AtcJ_{W89S}$ for AtcC is sufficient to allow residual in vivo interaction to sustain cold growth but with a more marked delay compared to the WT strain. This may account for the presence of alcohol residues (S and T) in some AtcJ homologues (Figure S4). In these bacteria, the residual AtcJ–AtcC interaction may be sufficient to sustain the function of the Atc system. Overall, these experiments demonstrate the crucial function of tryptophane to promote the AtcJ–AtcC interaction that is essential for growth at low temperature in *S. oneidensis*.

We investigated the literature to determine whether the organisms containing these JDPs (Table 1) are psychrophilic or show psychrotolerance capabilities. We found information for 18 out of 32 organisms. These 18 organisms are either characterised as psychrophilic or show the ability to grow at low temperature. For the others, it seems that the question of the behaviour towards cold was not addressed. However, it would be hazardous to associate the presence of the *atc* operon with a gain of function at low temperature. A more extensive study of the role of the *atc* operon on other organisms may or may not allow the generalisation of a link between *atc* genes and cold growth. Nevertheless, the role of AtcJ is indissociable from the presence of the three other Atc proteins. Indeed, AtcJ homologues are always encoded upstream of three other genes that seem in synteny and which encode for proteins predicted to be structurally related to AtcA, AtcB, and AtcC from *S. oneidensis*. In this organism, the expression of the *atc* operon is constitutive and of comparable level in the range of temperature 7–35°C, suggesting that it may be involved in other functions than cold adaptation (Maillot et al., 2019). Thus, AtcA, which is not important for cold growth, could be essential in other functions.

AtcB and AtcC, interacting with each other (Maillot et al., 2019), are predicted as globular proteins essentially containing alpha helices. The predicted structures of AtcB homologues are remarkably similar, suggesting a conserved function. For AtcC, however, although the N-terminal domains of AtcC homologues are predicted to have a similar fold (Figure 8C), the C-terminal domains greatly diverge in terms of size, sequence and model structure. This suggests that, as proposed for AtcJ, the N-terminal domains of AtcC harbour the interaction site with AtcB.

We observed variations in the probable operons containing the four *atc* genes. In some bacteria like *Moritella viscosa*, *Rhodoferax koreense*, or *Polaromonas naphtalenivorans*, the *atcC* gene is in probable transcriptional link with one or more other genes (Figure 7). We propose that this diversity determines the specificity of the function(s) of the Atc systems, which may go well beyond the ability to grow at low temperatures. Thus, AtcJ, A, B, and C may form a protein core that can be implemented by the other proteins to fulfil a dedicated DnaK- or HscA-dependent function depending on the organism. Complementation studies we performed on the *S. oneidensis* Δ*atcJ* strain showed that cold growth could be restored by production of exogenous AtcJ proteins from plasmid. AtcJs from *Collimonas pratensis* Ter91 and *Rhodoferax koreense* restored cold growth of but with a delay compared to the WT, whereas the protein from *Paraglaciecola psychrophila* did not (Figure S5). Whether these delays or non-complementation are the result of a protein production defect and/or low affinity of AtcJ proteins for AtcC remains to be determined, but these results suggest that the AtcJ–AtcC interaction, and more generally the DnaK(HscA)-AtcJ–AtcC interaction network, is a common feature of the functioning of the Atc system in organisms containing it. That AtcB interacts with the core RNA polymerase and probably

inhibits it (Maillot et al., 2021), could presume a function in gene expression regulation, but this remains to be demonstrated.

AUTHOR CONTRIBUTIONS

Lana Weber: Formal analysis (equal); investigation (equal); methodology (equal). **Atar Gilat:** Formal analysis (equal); investigation (equal); methodology (equal). **Nathanael Maillot:** Formal analysis (equal); investigation (equal); methodology (equal). **Deborah Byrne:** Formal analysis (equal); investigation (equal); methodology (equal); validation (equal). **Pascal Arnoux:** Conceptualization (equal); writing – review and editing (equal). **Marie-Thérèse Giudici-Orticoni:** Formal analysis (equal); writing – review and editing (equal). **Vincent Méjean:** Conceptualization (equal); formal analysis (equal); writing – review and editing (equal). **Marianne Ilbert:** Formal analysis (equal); investigation (equal); methodology (equal); validation (equal); writing – review and editing (equal). **Olivier Genest:** Conceptualization (equal); formal analysis (equal); investigation (equal); methodology (equal); project administration (equal); validation (equal); writing – review and editing (equal). **Rina Rosenzweig:** Conceptualization (equal); formal analysis (equal); investigation (equal); methodology (equal); validation (equal); writing – review and editing (equal). **Sébastien Dementin:** Conceptualization (equal); formal analysis (equal); investigation (equal); methodology (equal); project administration (equal); validation (equal); writing – original draft (equal); writing – review and editing (equal).

ACKNOWLEDGEMENTS

We thank the members of the Bip1 team for their help and suggestions during completion of this work. We thank Mathieu Rebeaud for helpful discussions related to the phylogeny of Atc proteins. We also thank Amane Kriach and Caroline Stemmler for their help on this project. The authors are thankful for the funding from Agence Nationale de la Recherche (ANR-16-CE11-0002-01, and ANR-19-CE44-0018), Aix-Marseille Université and the Centre National de la Recherche Scientifique.

CONFLICT OF INTEREST STATEMENT

The authors declare that they have no conflicts of interest with the contents of this article.

DATA AVAILABILITY STATEMENT

Data are available upon request.

ORCID

Vincent Méjean https://orcid.org/0000-0001-6533-5846
Sébastien Dementin https://orcid.org/0000-0001-6168-5371

REFERENCES

Abboud, R., Popa, R., Souza-Egipsy, V., Giometti, C.S., Tollaksen, S., Mosher, J.J. et al. (2005) Low-temperature growth of *Shewanella oneidensis* MR-1. *Applied and Environmental Microbiology*, 71, 811–816.

Baaziz, H., Gambari, C., Boyeldieu, A., Ali Chaouche, A., Alatou, R., Méjean, V. et al. (2017) ChrASO, the chromate efflux pump of *Shewanella oneidensis*, improves chromate survival and reduction. *PLoS One*, 12, e0188516.

Balchin, D., Hayer-Hartl, M. & Hartl, F.U. (2020) Recent advances in understanding catalysis of protein folding by molecular chaperones. *FEBS Letters*, 594, 2770–2781.

Baraquet, C., Théraulaz, L., Iobbi-Nivol, C., Méjean, V. & Jourlin-Castelli, C. (2009) Unexpected chemoreceptors mediate energy taxis towards electron acceptors in *Shewanella oneidensis*. *Molecular Microbiology*, 73, 278–290.

Barria, C., Malecki, M. & Arraiano, C.M. (2013) Bacterial adaptation to cold. *Microbiology*, 159, 2437–2443.

Barriot, R., Latour, J., Castanié-Cornet, M.-P., Fichant, G. & Genevaux, P. (2020) J-domain proteins in bacteria and their viruses. *Journal of Molecular Biology*, 432, 3771–3789.

Battesti, A. & Bouveret, E. (2012) The bacterial two-hybrid system based on adenylate cyclase reconstitution in *Escherichia coli*. *Methods*, 58, 325–334.

Bowman, J.P., McCammon, S.A., Nichols, D.S., Skerratt, J.H., Rea, S.M., Nichols, P.D. et al. (1997) *Shewanella gelidimarina* sp. nov. and *Shewanella frigidimarina* sp. nov., novel Antarctic species with the ability to produce eicosapentaenoic acid (20:5 omega 3) and grow anaerobically by dissimilatory Fe(III) reduction. *International Journal of Systematic Bacteriology*, 47, 1040–1047.

Brettar, I., Christen, R. & Höfle, M.G. (2002) *Shewanella denitrificans* sp. nov., a vigorously denitrifying bacterium isolated from the oxic-anoxic interface of the Gotland Deep in the central Baltic Sea. *International Journal of Systematic and Evolutionary Microbiology*, 52, 2211–2217.

Calloni, G., Chen, T., Schermann, S.M., Chang, H.-C., Genevaux, P., Agostini, F. et al. (2012) DnaK functions as a central hub in the *E. coli* chaperone network. *Cell Reports*, 1, 251–264.

Casanueva, A., Tuffin, M., Cary, C. & Cowan, D.A. (2010) Molecular adaptations to psychrophily: the impact of "omic" technologies. *Trends in Microbiology*, 18, 374–381.

Coates, J.D., Chakraborty, R., Lack, J.G., O'Connor, S.M., Cole, K.A., Bender, K.S. et al. (2001) Anaerobic benzene oxidation coupled to nitrate reduction in pure culture by two strains of *Dechloromonas*. *Nature*, 411, 1039–1043.

Coleman, N.V., Mattes, T.E., Gossett, J.M. & Spain, J.C. (2002) Biodegradation of cis-dichloroethene as the sole carbon source by a beta-proteobacterium. *Applied and Environmental Microbiology*, 68, 2726–2730.

Corpet, F. (1988) Multiple sequence alignment with hierarchical clustering. *Nucleic Acids Research*, 16, 10881–10890.

Craig, E.A. & Marszalek, J. (2017) How Do J-Proteins Get Hsp70 to Do So Many Different Things? *Trends in Biochemical Sciences*, 42, 355–368.

de Boer, W., Leveau, J.H.J., Kowalchuk, G.A., Gunnewiek, P.J.A.K., Abeln, E.C.A., Figge, M.J. et al. (2004) *Collimonas fungivorans* gen. nov., sp. nov., a chitinolytic soil bacterium with the ability to grow on living fungal hyphae. *International Journal of Systematic and Evolutionary Microbiology*, 54, 857–864.

de Maayer, P., Anderson, D., Cary, C. & Cowan, D.A. (2014) Some like it cold: understanding the survival strategies of psychrophiles. *EMBO Reports*, 15, 508–517.

Delaglio, F., Grzesiek, S., Vuister, G.W., Zhu, G., Pfeifer, J. & Bax, A. (1995) NMRPipe: a multidimensional spectral processing system based on UNIX pipes. *Journal of Biomolecular NMR*, 6, 277–293.

Dougherty, D.A. (1996) Cation-pi interactions in chemistry and biology: a new view of benzene, Phe, Tyr, and Trp. *Science*, 271, 163–168.

Dougherty, D.A. (2013) The cation-π interaction. *Accounts of Chemical Research*, 46, 885–893.

Emerson, D. & Moyer, C. (1997) Isolation and characterization of novel iron-oxidizing bacteria that grow at circumneutral pH. *Applied and Environmental Microbiology*, 63, 4784–4792.

Farh, M.E.-A., Kim, Y.-J., Singh, P., Jung, S.Y., Kang, J.-P. & Yang, D.-C. (2017) *Rhodoferax koreense* sp. nov, an obligately aerobic bacterium within the family *Comamonadaceae*, and emended description of the genus *Rhodoferax*. *Journal of Microbiology*, 55, 767–774.

Fauvet, B., Finka, A., Castanié-Cornet, M.-P., Cirinesi, A.-M., Genevaux, P., Quadroni, M. et al. (2021) Bacterial Hsp90 Facilitates the Degradation of Aggregation-Prone Hsp70-Hsp40 Substrates. *Frontiers in Molecular Biosciences*, 8, 653073.

Fernández, H., Prandoni, N., Fernández-Pascual, M., Fajardo, S., Morcillo, C., Díaz, E. et al. (2014) *Azoarcus* sp. CIB, an anaerobic biodegrader of aromatic compounds shows an endophytic lifestyle. *PLoS One*, 9, e110771.

Fessehaie, A. & Walcott, R.R. (2005) Biological control to protect watermelon blossoms and seed from infection by *Acidovorax avenae subsp. citrulli*. *Phytopathology*, 95, 413–419.

Fixen, K.R., Starkenburg, S.R., Hovde, B.T., Johnson, S.L., Deodato, C.R., Daligault, H.E. et al. (2016) Genome sequences of eight bacterial species found in coculture with the haptophyte *Chrysochromulina tobin*. *Genome Announcements*, 4, e01162-16.

Gallivan, J.P. & Dougherty, D.A. (1999) Cation-pi interactions in structural biology. *Proceedings of the National Academy of Sciences of the United States of America*, 96, 9459–9464.

Goddard, T.D., Huang, C.C., Meng, E.C., Pettersen, E.F., Couch, G.S., Morris, J.H. et al. (2018) UCSF ChimeraX: Meeting modern challenges in visualization and analysis. *Protein Science*, 27, 14–25.

Hau, H.H. & Gralnick, J.A. (2007) Ecology and biotechnology of the genus *Shewanella*. *Annual Review of Microbiology*, 61, 237–258.

Hwang, Y.J., Jang, G.I., Cho, B.C., Lee, J.I. & Hwang, C.Y. (2019) *Shewanella psychromarinicola* sp. nov., a psychrophilic bacterium isolated from pelagic sediment of the Ross Sea (Antarctica), and reclassification of *Shewanella arctica* Kim et al. 2012 as a later heterotypic synonym of *Shewanella frigidimarina* Bowman et al. 1997. *International Journal of Systematic and Evolutionary Microbiology*, 69, 2415–2423.

Jeon, C.O., Park, W., Ghiorse, W.C. & Madsen, E.L. (2004) *Polaromonas naphthalenivorans* sp. nov., a naphthalene-degrading bacterium from naphthalene-contaminated sediment. *International Journal of Systematic and Evolutionary Microbiology*, 54, 93–97.

Jeong, Y.-S., Song, S.-K., Lee, S.-J. & Hur, B.-K. (2006) The growth and EPA synthesis of *Shewanella oneidensis* MR-1 and expectation of EPA biosynthetic pathway. *Biotechnology and Bioprocess Engineering*, 11, 127–133.

Kalyuzhnaya, M.G., Beck, D.A.C., Vorobev, A., Smalley, N., Kunkel, D.D., Lidstrom, M.E. et al. (2012) Novel methylotrophic isolates from lake sediment, description of *Methylotenera versatilis* sp. nov. and emended description of the genus *Methylotenera*. *International Journal of Systematic and Evolutionary Microbiology*, 62, 106–111.

Kampinga, H.H. & Craig, E.A. (2010) The HSP70 chaperone machinery: J proteins as drivers of functional specificity. *Nature Reviews Molecular Cell Biology*, 11, 579–592.

Kanehisa, M. (2019) Toward understanding the origin and evolution of cellular organisms. *Protein Science*, 28, 1947–1951.

Kanehisa, M., Furumichi, M., Sato, Y., Ishiguro-Watanabe, M. & Tanabe, M. (2021) KEGG: integrating viruses and cellular organisms. *Nucleic Acids Research*, 49, D545–D551.

Kanehisa, M. & Goto, S. (2000) KEGG: kyoto encyclopedia of genes and genomes. *Nucleic Acids Research*, 28, 27–30.

Karimova, G., Pidoux, J., Ullmann, A. & Ladant, D. (1998) A bacterial two-hybrid system based on a reconstituted signal transduction pathway. *Proceedings of the National Academy of Sciences of the United States of America*, 95, 5752–5756.

Kim, H., Park, A.K., Lee, J.H., Kim, H.-W. & Shin, S.C. (2018) Complete genome sequence of *Colwellia hornerae* PAMC 20917, a cold-active enzyme-producing bacterium isolated from the Arctic Ocean sediment. *Marine Genomics*, 41, 54–56.

Kimbara, K., Hashimoto, T., Fukuda, M., Koana, T., Takagi, M., Oishi, M. et al. (1988) Isolation and characterization of a mixed culture that degrades polychlorinated biphenyls. *Agricultural and Biological Chemistry*, 52, 2885–2891.

Kluck, C.J., Patzelt, H., Genevaux, P., Brehmer, D., Rist, W., Schneider-Mergener, J. et al. (2002) Structure-function analysis of HscC, the *Escherichia coli* member of a novel subfamily of specialized Hsp70 chaperones. *The Journal of Biological Chemistry*, 277, 41060–41069.

Lange, O.F., Rossi, P., Sgourakis, N.G., Song, Y., Lee, H.-W., Aramini, J.M. et al. (2012) Determination of solution structures of proteins up to 40 kDa using CS-Rosetta with sparse NMR data from deuterated samples. *Proceedings of the National Academy of Sciences of the United States of America*, 109, 10873–10878.

Lemaire, O.N., Honoré, F.A., Tempel, S., Fortier, E.M., Leimkühler, S., Méjean, V. et al. (2019) *Shewanella decoloration-is* LDS1 chromate resistance. *Applied and Environmental Microbiology*, 85, e00777-19.

Lemaire, O.N., Méjean, V. & Iobbi-Nivol, C. (2020) The *Shewanella* genus: ubiquitous organisms sustaining and preserving aquatic ecosystems. *FEMS Microbiology Reviews*, 44, 155–170.

Lincoln, S.P., Fermor, T.R. & Tindall, B.J. (1999) *Janthinobacterium agaricidamnosum* sp. nov., a soft rot pathogen of *Agaricus bisporus*. *International Journal of Systematic Bacteriology*, 49, 1577–1589.

Maillot, N.J., Honoré, F.A., Byrne, D., Méjean, V. & Genest, O. (2019) Cold adaptation in the environmental bacterium *Shewanelle oneidensis* is controlled by a J-domain co-chaperone protein network. *Communications Biology*, 2, 323.

Maillot, N.J., Infossi, P., Dementin, S., Giudici-Orticoni, M.-T., Méjean, V. & Genest, O. (2021) Modulation of the RNA polymerase activity by AtcB, a protein associated with a DnaK chaperone network in *Shewanella oneidensis*. *Biochemical and Biophysical Research Communications*, 535, 66–72.

Makemson, J.C., Fulayfil, N.R., Landry, W., van Ert, L.M., Wimpee, C.F., Widder, E.A. et al. (1997) *Shewanella woodyi* sp. nov., an exclusively respiratory luminous bacterium isolated from the Alboran Sea. *International Journal of Systematic Bacteriology*, 47, 1034–1039.

Mayer, M.P. (2018) Intra-molecular pathways of allosteric control in Hsp70s. *Philosophical Transactions of the Royal Society of London. Series B, Biological Sciences*, 373, 20170183.

Mayer, M.P. (2021) The Hsp70-chaperone machines in bacteria. *Frontiers in Molecular Biosciences*, 8, 694012.

Mayer, M.P. & Gierasch, L.M. (2019) Recent advances in the structural and mechanistic aspects of Hsp70 molecular chaperones. *The Journal of Biological Chemistry*, 294, 2085–2097.

McGaughey, G.B., Gagné, M. & Rappé, A.K. (1998) pi-Stacking interactions. Alive and well in proteins. *The Journal of Biological Chemistry*, 273, 15458–15463.

Methé, B.A., Nelson, K.E., Deming, J.W., Momen, B., Melamud, E., Zhang, X. et al. (2005) The psychrophilic lifestyle as revealed by the genome sequence of *Colwellia psychrerythraea* 34H through genomic and proteomic analyses. *Proceedings of the National Academy of Sciences of the United States of America*, 102, 10913–10918.

Mirdita, M., Schütze, K., Moriwaki, Y., Heo, L., Ovchinnikov, S. & Steinegger, M. (2022) ColabFold—making protein folding accessible to all. *Nature Methods*, 19, 679–682.

Myeong, N.R., Seong, H.J., Kim, H.-J. & Sul, W.J. (2016) Complete genome sequence of antibiotic and anticancer agent violacein producing *Massilia* sp. strain NR 4-1. *Journal of Biotechnology*, 223, 36–37.

Peduzzi, S., Storelli, N., Welsh, A., Peduzzi, R., Hahn, D., Perret, X. et al. (2012) *Candidatus "Thiodictyon syntrophicum"*, sp. nov., a new purple sulfur bacterium isolated from the chemocline of Lake Cadagno forming aggregates and specific associations with *Desulfocapsa* sp. *Systematic and Applied Microbiology*, 35, 139–144.

Peoples, L.M., Kyaw, T.S., Ugalde, J.A., Mullane, K.K., Chastain, R.A., Yayanos, A.A. et al. (2020) Distinctive gene and protein characteristics of extremely piezophilic *Colwellia*. *BMC Genomics*, 21, 692.

Petriglieri, F., Singleton, C.M., Kondrotaite, Z., Dueholm, M.K.D., McDaniel, E.A., McMahon, K.D. et al. (2022) Reevaluation of the Phylogenetic Diversity and Global Distribution of the Genus "*Accumulibacter*". *mSystems*, 7, e0001622.

Pettersen, E.F., Goddard, T.D., Huang, C.C., Meng, E.C., Couch, G.S., Croll, T.I. et al. (2021) UCSF ChimeraX: Structure visualization for researchers, educators, and developers. *Protein Science*, 30, 70–82.

Rabus, R., Wöhlbrand, L., Thies, D., Meyer, M., Reinhold-Hurek, B. & Kämpfer, P. (2019) *Aromatoleum* gen. nov., a novel genus accommodating the phylogenetic lineage including *Azoarcus evansii* and related species, and proposal of *Aromatoleum aromaticum* sp. nov., *Aromatoleum petrolei* sp. nov., *Aromatoleum bremense* sp. nov., *Aromatoleum toluolicum* sp. nov. and *Aromatoleum diolicum* sp. nov. *International Journal of Systematic and Evolutionary Microbiology*, 69, 982–997.

Robert, X. & Gouet, P. (2014) Deciphering key features in protein structures with the new ENDscript server. *Nucleic Acids Research*, 42, W320–W324.

Rosenzweig, R., Nillegoda, N.B., Mayer, M.P. & Bukau, B. (2019) The Hsp70 chaperone network. *Nature Reviews Molecular Cell Biology*, 20, 665–680.

Serlidaki, D., van Waarde, M.A.W.H., Rohland, L., Wentink, A.S., Dekker, S.L., Kamphuis, M.J. et al. (2020) Functional diversity between HSP70 paralogs caused by variable interactions with specific co-chaperones. *The Journal of Biological Chemistry*, 295, 7301–7316.

Shen, Y., Delaglio, F., Cornilescu, G. & Bax, A. (2009) TALOS+: a hybrid method for predicting protein backbone torsion angles from NMR chemical shifts. *Journal of Biomolecular NMR*, 44, 213–223.

Shen, Y., Lange, O., Delaglio, F., Rossi, P., Aramini, J.M., Liu, G. et al. (2008) Consistent blind protein structure generation from NMR chemical shift data. *Proceedings of the National Academy of Sciences of the United States of America*, 105, 4685–4690.

Singleton, D.R., Ramirez, L.G. & Aitken, M.D. (2009) Characterization of a polycyclic aromatic hydrocarbon degradation gene cluster in a phenanthrene-degrading *Acidovorax* strain. *Applied and Environmental Microbiology*, 75, 2613–2620.

Song, C., Schmidt, R., de Jager, V., Krzyzanowska, D., Jongedijk, E., Cankar, K. et al. (2015) Exploring the genomic traits of fungus-feeding bacterial genus *Collimonas*. *BMC Genomics*, 16, 1103.

Tunsjø, H.S., Paulsen, S.M., Mikkelsen, H., L'abée-Lund, T.M., Skjerve, E. & Sørum, H. (2007) Adaptive response to environmental changes in the fish pathogen *Moritella viscosa*. *Research in Microbiology*, 158, 244–250.

Ulrich, L., Giez, C., Steiner, L.X., Hentschel, U. & Lachnit, T. (2022) Adaptive lifestyle of bacteria determines phage-bacteria interaction. *Frontiers in Microbiology*, 13, 1056388.

Uroz, S., Tech, J.J., Sawaya, N.A., Frey-Klett, P. & Leveau, J.H.J. (2014) Structure and function of bacterial communities in ageing soils: Insights from the Mendocino ecological staircase. *Soil Biology and Biochemistry*, 69, 265–274.

Vranken, W.F., Boucher, W., Stevens, T.J., Fogh, R.H., Pajon, A., Llinas, M. et al. (2005) The CCPN data model for NMR spectroscopy: development of a software pipeline. *Proteins*, 59, 687–696.

Walsh, P., Bursać, D., Law, Y.C., Cyr, D. & Lithgow, T. (2004) The J-protein family: modulating protein assembly, disassembly and translocation. *EMBO Reports*, 5, 567–571.

Xu, X., Tian, L., Zhang, S., Jiang, L., Zhang, Z. & Huang, H. (2019) Complete genome sequence of *Janthinobacterium sp. B9-8*, a violacein-producing bacterium isolated from low-temperature sewage. *Microbial Pathogenesis*, 128, 178–183.

Yakimov, M.M., Giuliano, L., Gentile, G., Crisafi, E., Chernikova, T.N., Abraham, W.-R. et al. (2003) *Oleispira antarctica* gen. nov., sp. nov., a novel hydrocarbonoclastic marine bacterium isolated from Antarctic coastal sea water. *International Journal of Systematic and Evolutionary Microbiology*, 53, 779–785.

Zeng, Z., Liu, X., Yao, J., Guo, Y., Li, B., Li, Y. et al. (2016) Cold adaptation regulated by cryptic prophage excision in *Shewanella oneidensis*. *The ISME Journal*, 10, 2787–2800.

Zhang, D.-C., Yu, Y., Chen, B., Wang, H.-X., Liu, H.-C., Dong, X.-Z. et al. (2006) *Glaciecola psychrophila* sp. nov., a novel psychrophilic bacterium isolated from the Arctic. *International Journal of Systematic and Evolutionary Microbiology*, 56, 2867–2869.

Zhang, Y. & Gross, C.A. (2021) Cold shock response in bacteria. *Annual Review of Genetics*, 55, 377–400.

SUPPORTING INFORMATION

Additional supporting information can be found online in the Supporting Information section at the end of this article.

How to cite this article: Weber, L., Gilat, A., Maillot, N., Byrne, D., Arnoux, P., Giudici-Orticoni, M.-T. et al. (2023) Bacterial adaptation to cold: Conservation of a short J-domain co-chaperone and its protein partners in environmental proteobacteria. *Environmental Microbiology*, 1–18. Available from: https://doi.org/10.1111/1462-2920.16478